buildings

MDPI

Article

Design and Experimental Analysis of Seismic Isolation Bearings for Nuclear Power Plant Containment Structures

Qiang Pei [1,†], Pengfei Qi [1,†], Zhicheng Xue [2,3,*,†], Jintu Zhong [2] and Yao Zhang [3]

[1] College of Civil Engineering and Architecture, Dalian University, Dalian 116622, China; peiqiang@dlu.edu.cn (Q.P.)
[2] Architecture and Civil Engineering Institute, Guangdong University of Petrochemical Technology, Maoming 525000, China
[3] School of Architecture and Civil Engineering, Heilongjiang University of Science and Technology, Harbin 150020, China
* Correspondence: xuezhicheng0630@163.com
† These authors contributed equally to this work.

Abstract: The aim of this study was to further research the mechanical properties of epoxy thick-layer rubber isolation bearings, adopting orthogonal design and efficacy coefficient methods in order to optimize the geometric dimensions and material parameters of the bearing, summarizing the influence of various factors on the overall performance indicators of the bearing, and determining the optimal plan through parameter adjustment. Through a combination of experiments and simulations, the fundamental characteristics of epoxy thick-layer rubber isolation bearings are studied to determine the influence law of vertical pressure on their horizontal stiffness, vertical stiffness, and damping ratio. The analysis results suggest that epoxy plate thick-layer rubber isolation bearing exhibits stable deformation ability and possesses distinctive damping characteristics. Furthermore, it is observed that the horizontal stiffness of these bearings gradually diminishes as the vertical pressure increases. When the shear displacement reaches 80 mm, there is a notable strengthening effect observed in the horizontal stiffness of the bearing. This strengthening phenomenon proves advantageous in preventing damage to the bearing due to excessive displacement; furthermore, it is noteworthy that the vertical stiffness and damping ratio of the bearing increased with the rise in vertical pressure.

Keywords: nuclear power plant containment structure; epoxy board thick-layer rubber isolation bearing; 3D isolation; seismic performance

Citation: Pei, Q.; Qi, P.; Xue, Z.; Zhong, J.; Zhang, Y. Design and Experimental Analysis of Seismic Isolation Bearings for Nuclear Power Plant Containment Structures. *Buildings* **2023**, *13*, 2366. https://doi.org/10.3390/buildings13092366

Academic Editor: Marco Di Ludovico

Received: 17 August 2023
Revised: 2 September 2023
Accepted: 4 September 2023
Published: 17 September 2023

1. Introduction

Although the application prospects of nuclear power are considerable, the issue of nuclear radiation has also attracted the attention of people from all walks of life. On 16 July 2007, an earthquake measuring 6.8 on the Richter scale occurred in Niigata Prefecture, Japan, causing damage to the maintenance structure of the world's largest nuclear power plant, Kashizaki Moyu, and causing water leakage containing trace amounts of radioactive substances such as iodine and cesium. On 11 March 2011, the Fukushima nuclear power plant in Japan was affected by a magnitude 9.0 earthquake, resulting in a major nuclear leakage accident [1–3]. The uncertainty of earthquakes poses a huge threat to the construction and use of nuclear power plants. As a safety guarantee for nuclear power use, how to effectively enhance the seismic bearing capacity of nuclear power structures and improve their safety margin to make nuclear power facilities withstand the test of earthquakes has attracted widespread attention from experts [4–8].

In recent years, the base isolation system has been rapidly developed and applied as a technical means to protect the overall safety of structures, from civil buildings, various industrial buildings, and bridges to important infrastructure, including nuclear power plant engineering facilities and structures, and has achieved numerous research results [9–15].

Pan et al. conducted experimental research on the isolation effect of four types of laminated rubber bearings and found that the isolation effect and stability of thick natural rubber bearings and thick high damping rubber bearings were superior to those of thin rubber bearings [16]. Due to the lack of deformation capacity of the isolation layer under rare earthquakes, Wu et al. proposed a new type of isolation bearing and simulated it to improve the deformation capacity of the overall structure. The results showed that the structure still has sufficient energy dissipation capacity under extremely rare earthquakes [17]. However, earlier studies focused on horizontal isolation systems and ignored the influence of seismic motion in the vertical direction. With the improvement of isolation systems, many experts and scholars began to focus on three-dimensional isolation systems [18–20]. Liang et al. proposed and tested three-dimensional isolation bearings and found that they can effectively isolate horizontal and vertical ground motions [21]. Zhang et al. designed a three-dimensional hybrid isolation system and applied it to large-span spatial structures, confirming that the three-dimensional hybrid isolation system can not only extend the natural vibration period of the structure, but also effectively disperse seismic energy in three directions [22]. Han et al. proposed a new type of air spring friction pendulum system (FPS) three-dimensional isolation bearing and conducted mechanical tests. The results showed that the bearing with lower vertical stiffness can effectively isolate long-term ground vibration [23]. Different isolation systems and the material characteristics of isolation bearings can have an impact on the isolation effect [24–28]. Zhang et al. mainly studied the seismic performance of rubber isolation bearings and found that natural rubber bearings have good isolation effects [29]. Yuan et al. designed a steel damper reinforced polyurethane bearing for structural seismic resistance, and subsequently conducted quasi-static compression, friction, and cyclic shear tests and found that the bearing has high strength and energy dissipation capacity [30]. With the diversified development of society, limited isolation bearing structures are not suitable for the isolation and vibration reduction in intelligent transportation buildings. Peng et al. analyzed the grid shell structure of isolation bearings based on intelligent transportation of sensor networks. By increasing the flexibility of the system and appropriate damping, it can effectively avoid the upward transmission of ground vibrations [31]. However, with the increasing industrial production worldwide, building structures are more susceptible to direct threats caused by accidents, explosions, seismic effects, etc. Therefore, the seismic isolation performance of nuclear containment structures needs to be put on the agenda as soon as possible [32,33].

The above research results fully demonstrate that the development of isolation technology is relatively mature. In order to fully understand the mechanical properties of epoxy thick-layer rubber isolation bearings, this article uses the FR-4 epoxy resin board with low density, high strength, strong plasticity, and relatively low cost to replace the steel plate of the support reinforcement layer, and the orthogonal design method and efficacy coefficient method were used to optimize the design. Then, through experimental loading and numerical simulation, the basic performance of the epoxy plate thick-layer rubber isolation bearing was studied, and the feasibility of the designed three-dimensional isolation bearing was explored. The results showed that the epoxy plate thick-layer rubber isolation bearing has strong damping characteristics, which is beneficial for the isolation and energy consumption of the structure under earthquake action.

2. Optimization Design of Epoxy Plate Thick-Layer Rubber Isolation Bearings

2.1. Determination of Optimization Indicators for Epoxy Plate Thick-Layer Rubber Isolation Bearings

In order to improve the horizontal and vertical isolation performance of epoxy thick-layer rubber isolation bearings, it is necessary to design the horizontal stiffness, buckling stress, and vertical stiffness of the bearings reasonably. Under the action of compression and shear, due to the phenomenon of stress concentration in the reinforcement layer of the bearing, which affects the overall safety of the bearing during use, two optimization measures are usually taken: one is to improve the material strength of the reinforcement layer, and the other is to control the generated concentrated stress. Therefore, the horizontal

stiffness, vertical stiffness, buckling stress, and maximum concentrated stress under shear compression of the bearing are used as control indicators.

2.1.1. Horizontal Stiffness of Rubber Isolation Bearings

The calculation of the horizontal stiffness of laminated rubber isolation bearings can be regarded as a compression bending rod under the simultaneous action of compression, bending, and shear. According to Hiringx theory [34], the formula for calculating the horizontal stiffness is:

$$K_h = \frac{P^2}{2k_r qtan(qH/2) - PH} \tag{1}$$

P: compressive load (N);
H: total thickness of rubber layer and sandwich thin steel plate (mm);
q: bearing stiffness conversion coefficient, $q = \sqrt{\frac{P}{k_r}(1 + \frac{P}{k_s})}$;
k_r: effective shear stiffness of the bearing (N/mm), $k_r = E_{rb} I \frac{H}{T_R}$, $E_{rb} = \frac{E_r E_b}{E_r + E_b}$;
k_s: effective bending stiffness of the bearing (N/mm), $k_s = GA\frac{H}{T_R}$;
E_r: bending elastic modulus of rubber (N/mm), $E_r = 3G(1 + \frac{2}{3}k{S_1}^2)$
When the vertical pressure is 0, the horizontal stiffness of the rubber isolation bearing is:

$$K_h = \frac{GA}{T_R} = \frac{G\pi}{4} \times \frac{D^2 - {D_0}^2}{nt_r} \tag{2}$$

G: shear modulus of rubber; A: effective cross-sectional area of the bearing;
T_R: total thickness of the rubber layer; D: effective diameter of the bearing;
D_0: opening diameter of the bearing; N: number of rubber layers of the bearing;
t_r: single layer thickness of the rubber layer of the bearing; S_1: the first shape coefficient of the bearing.

2.1.2. Vertical Stiffness of Rubber Isolation Bearings

The vertical stiffness K_v of the rubber bearing is:

$$K_v = \frac{E_{cb} A}{T_R} \tag{3}$$

E_{cb}: Corrected compressive modulus of elasticity (MPa), $E_{cb} = \frac{E_c E_b}{E_c + E_b}$;
E_c: apparent elastic modulus of bearing rubber (MPa), $E_c = E_0(1 + 2k{S_1}^2)$;
E_b: bulk modulus of rubber (MPa);
E_0: elastic modulus of rubber (MPa);
k: hardness correction coefficient;
S_1: first shape coefficient of the bearing, $S_1 = \frac{D - D_0}{4t_r}$.

2.1.3. Buckling Stress of Rubber Isolation Bearings

The buckling load P_{cr} is:

$$P_{cr} = \frac{1}{2}k_s \left[\sqrt{1 + \frac{4P^2 k_r}{H^2 k_s}} - 1 \right] \tag{4}$$

Substitute k_s and k_r into the above equation to calculate the buckling stress of the bearing σ_{cr}:

$$\sigma_{cr} = \frac{P_{cr}}{A} \tag{5}$$

Safety factor when using the bearing λ for:

$$\lambda = \frac{\sigma_0}{\sigma_{cr}} \tag{6}$$

σ_0: axial pressure used in the design of rubber isolation bearings (MPa).

2.1.4. Concentrated Stress of Epoxy Plate Thick-Layer Rubber Isolation Bearings under Compressive Shear Action

Using the finite element software ABAQUS to establish a three-dimensional finite element model of the bearing and simulate compression shear tests, it is possible to intuitively understand the stress state of each part of the bearing, thereby determining the maximum concentrated stress.

1. Geometric dimensions of the bearing

The main materials of epoxy thick-layer rubber isolation bearings are rubber, FR-4 epoxy resin plate, and steel plate. The total height of the bearing is 220 mm, and the thickness of both connecting plates is 20 mm. The thickness of the upper and lower sealing plates is 12 mm. The reinforcing layer of each layer is made of FR-4 epoxy resin plate with a thickness of 6mm, and the rubber thickness of each layer is 12 mm. FR-4 epoxy resin board can be simplified as an elastic material, with a Young's modulus of 17,420 MPa and a Poisson's ratio of 0.3. The connecting plate is a square Q235 steel plate with bolt holes at four corners and a side length of 385 mm. The Young's modulus is 200,000 MPa, the yield strength is 235 MPa, and the Poisson's ratio is 0.3. The outer diameter and inner diameter of the sealing plate, stiffening layer FR-4 epoxy resin plate, and rubber layer are 250 mm and 50 mm, and the bearing is covered with a 6 mm rubber protective layer around it. The sealing plate and connecting plate are made of Q235 steel, and the shear modulus of rubber is 0.5 MPa. The geometric dimensions of the isolation bearing are shown in Figure 1.

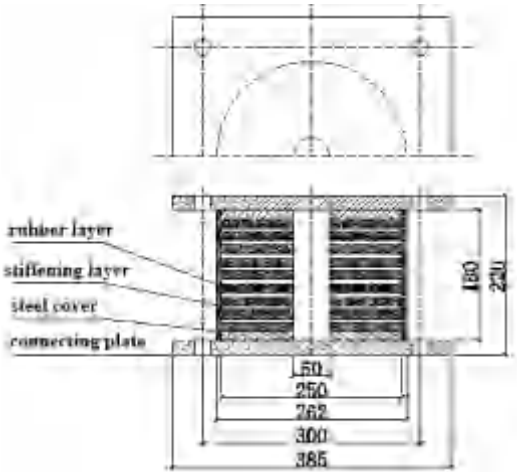

Figure 1. Epoxy resin board thick rubber isolation bearing diagram.

2. Selection and parameter determination of rubber constitutive model

In the epoxy thick-layer rubber isolation bearing, the Mooney–Rivlin model is selected to simulate the stress–strain of the rubber layer inside the bearing. Assuming the rubber material as an incompressible material and taking the volume ratio J before and after deformation as 1, the strain energy function of the model is:

$$U = C_{10}(I_1 - 3) + C_{01}(I_2 - 3) \tag{7}$$

C_{10} and C_{01}: the two parameters of the Mooney–Rivlin model;
I_1 and I_2 are the first and second invariants, respectively.

The elastic modulus E of rubber and the shear modulus G of rubber have the following relationship:

$$G = \frac{E}{2(1+\mu)} \tag{8}$$

Due to the incompressibility of rubber, the Poisson's ratio μ if the value is 0.5, then $E = 3G$, and the relationship between G or E and the material constant is:

$$G = 2(C_{10} + C_{01}) \tag{9}$$

$$E = 6C_{10}(1 + \frac{C_{01}}{C_{10}}) \tag{10}$$

Based on the shear modulus of rubber isolation bearings G = 0.5 MPa, assuming C_{01} = 0.25 C_{10}, Formula (9) yields 2 (C_{10} + 0.25 C_{10}) = G, which means $C_{10} = G/(2 \times 1.25)$; therefore, C_{10} = 0.2 MPa, C_{01} = 0.05 MPa.

Considering the compressibility of rubber materials under compression, it can be reflected by the Mooney–Rivlin model constant D_1. Generally, the bulk modulus E of rubber is taken as 2000 MPa, and D_1 is related to the bulk modulus [35]: $D_1 = 2/E = 0.001$ (MPa)$^{-1}$.

3. Establishing a finite element model

Based on the dimensions shown in Figure 1, establish a mesh divided model as shown in Figure 2. Due to the fact that the connecting plate is not perforated, while the sealing plate, the reinforcing layer FR-4 epoxy resin plate, and the rubber layer are perforated (with a diameter of 50 mm), the bearing model is established in two parts. Bind and connect the upper and lower sealing plates with the upper and lower connecting plates. The steel plate and FR-4 epoxy resin board are made of C3D8 units; rubber, on the other hand, uses C3D8H units.

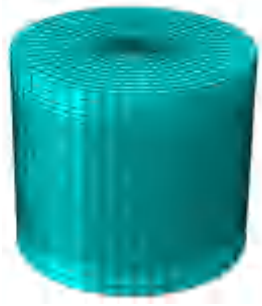

Figure 2. Epoxy resin board thick rubber bearing model.

4. The stress state of compression shear simulation

The first analysis step is to set the duration to 1 s, and complete the vertical loading within 1 s. The Mises stress distribution of the bearing under axial compression is shown in Figure 3; The second analysis step is set with a duration of 314 s and a loading frequency of 0.02 Hz. Three cycles of loading are completed within 314 s. Under shear compression, the Mises stress distribution of the horizontal displacement of the bearing is shown in Figure 4.

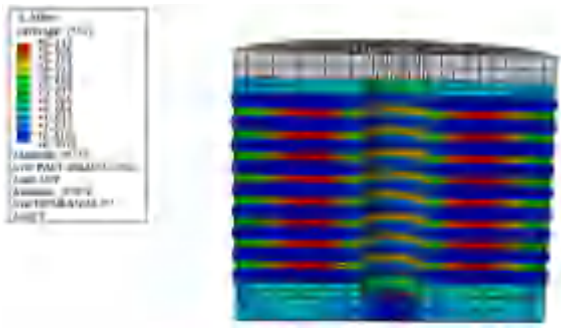

Figure 3. Mises stress distribution of the bearing under axial compression.

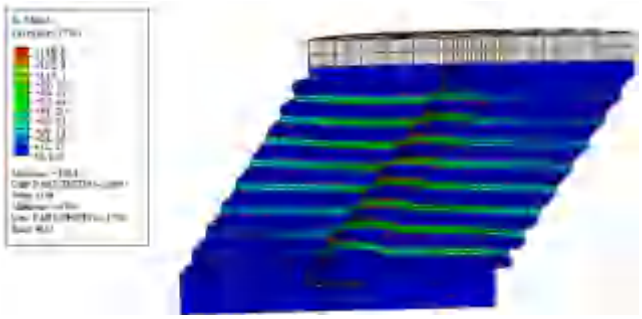

Figure 4. Mises stress distribution of the bearing under compression and shear.

As shown in Figures 3 and 4, the concentrated stress under axial compression occurs at a distance of 1/3 from the opening. With the application of horizontal displacement, stress concentration gradually develops to the center of the bearing. Stress concentration is an important factor affecting the bearing capacity of bearings, and the failure of bearings often leads to the inability of the stiffening layer to withstand the lateral tension caused by rubber expansion, leading to instability or tearing.

2.2. Optimization Design of Epoxy Plate Thick-Layer Rubber Isolation Bearings

Referring to the parameters of existing epoxy plate thick-layer rubber isolation bearings, a preliminary selection of bearing diameter (D) of 250 mm and a total height of 220 mm has been made. When the diameter and height of the bearing are constant, the diameter of the opening (D_0) is taken as 30 mm, 40 mm, 50 mm, and 60 mm, respectively. The ratio of the thickness of the rubber layer to the stiffener layer (δ) is not greater than 3.0, usually taken as 2.0. To ensure that the bearing has a large deformation capacity, the thickness ratio is taken as 1.5, 2.0, 2.5, and 3.0, respectively, and the number of rubber layers (n) is taken as 9, 10, 11, and 12, respectively. The shear modulus of rubber (G) should not be too large, taking 1.0 MPa, 1.1 MPa, 1.2 MPa, and 1.3 MPa, respectively. Using the orthogonal design method, the influence factors of the epoxy plate thick-layer rubber isolation bearing were analyzed, including the opening diameter, shear modulus of rubber, thickness ratio of rubber layer to stiffening layer, and number of rubber layers. Four levels were set for each factor, and the L_{16} (4^4) orthogonal table was selected. The bearing performance analysis of 16 schemes was carried out sequentially, as shown in Table 1.

Table 1. Factor level of the first round of the thick rubber isolation bearing.

Scheme	D_0 (mm)	G (MPa)	δ	n
1	30	1.0	1.5	9
2	30	1.1	2.0	10
3	30	1.2	2.5	11
4	30	1.3	3.0	12
5	40	1.0	2.0	11
6	40	1.1	1.5	12
7	40	1.2	3.0	9
8	40	1.3	2.5	10
9	50	1.0	2.5	12
10	50	1.1	3.0	11
11	50	1.2	1.5	10
12	50	1.3	2.0	9
13	60	1.0	3.0	10
14	60	1.1	2.5	9
15	60	1.2	2.0	12
16	60	1.3	1.5	11

The efficacy coefficient method is a research method that optimizes the selection of multiple indicators based on scheme design. Assuming there are m indicator values $f_i(x)$,

calculate the corresponding efficacy coefficient y_i for each indicator value obtained for each design scheme, where $i = 1, 2, \ldots, m$. Based on each efficacy coefficient value, obtain the total efficacy coefficient Y:

$$Y = \sqrt[m]{y_1 y_2 \cdots y_m} \tag{11}$$

In the above equation, the total efficacy coefficient Y reflects the overall advantages and disadvantages of m indicators, and the larger the coefficient value, the more the scheme design meets the design requirements. For the analysis of a certain indicator, the larger y_i, the better. fmax and fmin represent the maximum and minimum values among all schemes, then y_i is:

$$y_i = 0.4 \times \frac{(f_i - f_{\min})}{(f_{\max} - f_{\min})} + 0.6 \tag{12}$$

On the contrary, when a certain indicator is smaller and better, y_i can be calculated according to the following equation:

$$y_i = 0.4 \times \frac{(f_i - f_{\max})}{(f_{\min} - f_{\max})} + 0.6 \tag{13}$$

Determine the plan based on the efficacy coefficient method, and then continue to optimize on this basis until the optimal plan is obtained. The results of the first round of efficacy coefficient are shown in Table 2.

Table 2. Corresponding control index values and total efficacy factors of 16 schemes (first round).

Scheme	Buckling Stress (MPa)	Maximum Shear Stress (MPa)	K_h (kN/mm)	K_v (kN/mm)	Y
1	15.207	178.80	0.494	76.227	0.835
2	15.387	199.30	0.495	72.381	0.780
3	16.666	171.50	0.507	82.482	0.793
4	18.856	229.10	0.526	100.246	0.719
5	14.839	176.70	0.446	77.837	0.846
6	21.646	191.40	0.543	127.195	0.819
7	12.077	266.30	0.477	43.733	0.752
8	16.541	229.60	0.542	71.669	0.762
9	13.735	241.50	0.413	68.763	0.813
10	12.684	217.60	0.433	51.558	0.774
11	19.258	145.80	0.580	88.802	0.829
12	16.223	196.70	0.567	62.600	0.788
13	10.135	241.70	0.385	37.264	0.783
14	10.975	226.60	0.442	35.151	0.801
15	18.379	188.70	0.519	85.590	0.800
16	23.158	152.80	0.619	111.985	0.783

Based on the orthogonal design table, sensitivity analysis was conducted on factors such as the bearing opening diameter, rubber shear modulus, the thickness ratio of rubber layer to stiffener layer, and the number of rubber layers. The analysis results are shown in Table 3.

From Table 2, it can be seen that the sensitivity of factors affecting the seismic isolation performance of bearings is ranked from high to low: opening diameter, rubber shear modulus, thickness ratio of rubber layer to stiffener layer, and number of rubber layers. According to Table 3, Scheme 5 is the optimal solution. To further optimize the design, the hole diameters of 30 mm, 40 mm, and 50 mm were reselected, and the rubber shear modulus was 1.0 MPa, 1.1 MPa, and 1.2 MPa. The thickness ratio of the rubber layer to the stiffener layer was 1.5, 2.0, and 2.5, and the number of rubber layers was 10, 11, and 12. An optimization problem with three factors and three levels was established, the orthogonal table L_9 (3^3) was selected, and the optimal result of the first round of optimization design

was recorded as Scheme 5a. The total efficacy coefficient calculation results are shown in Table 4.

Table 3. Results of L_{16} (4^4) multi-factor orthogonal sensitivity analysis.

Scheme	D_0 (mm)	G (MPa)	δ	n	Y
1	30	1.0	1.5	9	0.835
2	30	1.1	2.0	10	0.780
3	30	1.2	2.5	11	0.793
4	30	1.3	3.0	12	0.719
5	40	1.0	2.0	11	0.846
6	40	1.1	1.5	12	0.819
7	40	1.2	3.0	9	0.752
8	40	1.3	2.5	10	0.762
9	50	1.0	2.5	12	0.813
10	50	1.1	3.0	11	0.774
11	50	1.2	1.5	10	0.829
12	50	1.3	2.0	9	0.788
13	60	1.0	3.0	10	0.783
14	60	1.1	2.5	9	0.801
15	60	1.2	2.0	12	0.800
16	60	1.3	1.5	11	0.783
K1	0.816	0.819	0.782	0.794	
K2	0.803	0.794	0.795	0.788	
K3	0.792	0.793	0.801	0.799	
K4	0.757	0.763	0.792	0.788	
R	0.059	0.056	0.019	0.011	

K represents the average value, 1–4 are four influencing factors: opening diameter, rubber shear modulus, thickness ratio of rubber layer to stiffener layer, and number of rubber layers; R represents range.

Table 4. Corresponding control indicators and total efficacy factors of 9 schemes (second round).

Scheme	Buckling Stress (MPa)	Maximum Shear Stress (MPa)	K_h (kN/mm)	K_v (kN/mm)	Y
1	16.960	114.70	0.496	94.802	0.851
2	16.947	168.10	0.496	87.896	0.818
3	18.182	226.70	0.509	98.349	0.733
4	16.205	176.00	0.447	92.909	0.816
5	13.089	220.20	0.459	54.229	0.781
6	22.075	138.30	0.591	120.655	0.755
7	12.598	212.40	0.412	57.740	0.785
8	20.818	144.50	0.535	113.901	0.777
9	15.910	193.90	0.526	66.536	0.769
5a	13.181	142.10	0.446	77.837	0.818

From Table 4, it can be seen that in the second round of optimization, Scheme 1 has the highest total efficiency coefficient and the best comprehensive performance of the bearing. Continue to optimize the design and determine the third round of the plan. The opening diameters are 0 mm, 10 mm, and 20 mm, respectively. The rubber shear modulus is 1.0 MPa, 1.1 MPa, and 1.2 MPa. The thickness ratio of the rubber layer to the stiffener layer is 1.5, 2.0, and 3.0, and the number of rubber layers is 9, 10, and 11. Select the orthogonal table L_9 (3^3) and calculate the total efficacy coefficient. The optimal solution for the second round is denoted as 1b, and the calculation results are shown in Table 5.

After calculation and comparison, Scheme 1 in the third round of optimization results is the best (D_0 = 0mm, G = 1.0 MPa, δ = 1.5, n = 9). By comparing the results of various schemes in the optimization design process, it was found that the stability of the epoxy plate thick-layer rubber isolation bearing without holes was significantly improved compared to the bearings with holes, and the concentrated stress was significantly reduced. The reasonable selection of rubber materials can reduce the horizontal and vertical stiffness of

epoxy thick-layer rubber isolation bearings. The hardness of rubber materials should not be too small, as too small can lead to a significant decrease in the bearing's restoring force, thereby affecting the safe use of the bearing. The thickness ratio of the rubber layer to the stiffener layer and the number of rubber layers have little effect on the results; thus, further optimization is not necessary.

Table 5. Corresponding control indicators and total efficacy factors of 9 schemes (third round).

Scheme	Buckling Stress (MPa)	Maximum Shear Stress (MPa)	K_h (kN/mm)	K_v (kN/mm)	Y
1	17.041	43.70	0.501	99.125	0.832
2	17.242	52.31	0.502	94.140	0.787
3	18.681	60.73	0.515	107.361	0.759
4	16.644	83.47	0.457	103.453	0.806
5	13.181	105.30	0.468	58.098	0.773
6	22.440	71.59	0.603	131.740	0.726
7	12.832	157.50	0.425	64.607	0.809
8	21.376	93.52	0.552	129.503	0.812
9	16.015	120.80	0.542	72.765	0.735
1b	16.960	114.70	0.496	94.802	0.775

2.3. Optimization Design Results of Epoxy Plate Thick-Layer Rubber Isolation Bearings

According to the optimized design through litigation, the design diagram of the epoxy plate thick-layer rubber isolation bearing is shown in Figure 5, and the specific parameters of the bearing are shown in Table 6.

Table 6. Size table of epoxy resin board thick rubber isolation bearing.

Name		Parameter Value
rubber	shear modulus (G)/MPa	1.0
	elastic modulus (E_0)/MPa	5.1
	bulk modulus (E_∞)/MPa	2160
	rubber correction coefficient (k)	0.874
rubber layer	Thickness (t_r)/mm	10.88
	Number (n)	9
	total thickness (T_R)/mm	97.92
internal epoxy resin board	thickness (t_f)/mm	7.26
	number ($n-1$)	8
	total thickness (T_f)/mm	58.08
design axial pressure/kN		300
design stress/MPa		6.37
first shape coefficient (S_1)		5.74
second shape coefficient (S_2)		2.55
effective diameter of bearing (D)/mm		250
thickness of protective layer rubber/mm		12
thickness of upper and lower sealing plates/mm		12
thickness of connecting plate/mm		20
total height of bearing/mm		220
horizontal stiffness/(kN/mm)		0.501
vertical stiffness/(kN/mm)		99.125
buckling stress/MPa		17.041

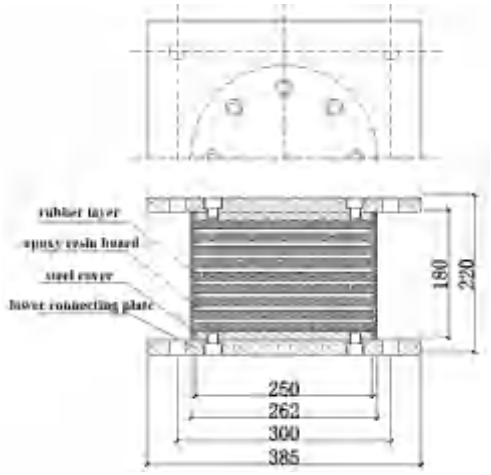

Figure 5. Design diagram of epoxy resin board thick rubber isolation bearing.

3. Experimental and Numerical Simulation Study on Mechanical Properties of Epoxy Plate Thick-Layer Rubber Isolation Bearings

Based on the optimization design results of epoxy thick-layer rubber isolation bearings, the adhesive strength between rubber and epoxy resin plates was tested, referring to the specification [36]. The vertical stiffness of the bearing under different vertical pressures and the horizontal stiffness of different shear strains under different vertical pressures were measured using a compression shear testing machine. At the same time, a three-dimensional finite element model of epoxy thick-layer rubber isolation bearings was established, and the internal stress state of the bearings was analyzed.

3.1. Adhesion Strength Test of Rubber and Epoxy Resin Board

The adhesive strength test between rubber and epoxy resin board can be found in the specification [37]. Six sets of test pieces were made in order to bond rubber sheets with epoxy resin plates. The surfaces of the epoxy resin plates on test pieces 1–3 were not polished, while the surfaces of the oxygen resin plates on test pieces 4–6 were polished. Then, an electronic universal testing machine was used as shown in Figure 6 for experimental loading. During the test, a 90° angle should be maintained between the tensile direction of the rubber sheet and the surface of the epoxy resin board; the loading speed of the tensile force of the testing machine is 50 mm/min.

Figure 6. Electronic universal testing machine.

The test results are calculated using the following formula for peel adhesion strength:

$$\sigma = \frac{F}{B} \tag{14}$$

B: sample width, mm;

σ: peel bonding strength, N/mm;
F: maximum peeling force, N.

The test results are represented by the average, maximum, and minimum values of three specimens, and the calculation results are shown in Table 7.

Table 7. Peel adhesion strength of rubber sheet and epoxy resin sheet.

Sample Number	Specimen Width (mm)	Maximum Peeling Force (N)	Peel Bonding Strength (N/mm)	Mean Peel Adhesion Strength (N/mm)
1	25	138.25	5.53	
2	25	140.75	5.64	5.55
3	25	137.25	5.49	
4	25	208.50	8.34	
5	25	206.25	8.25	8.35
6	25	211.50	8.44	

According to the specifications [38,39], the adhesive strength between the epoxy resin board and the rubber is $\sigma \geq 6$ N/mm. Therefore, the adhesive strength between the epoxy resin board and the rubber meets the requirements.

3.2. Mechanical Performance Test of Epoxy Plate Thick-Layer Rubber Isolation Bearing

3.2.1. Test Model

Based on the specific parameters of the optimized epoxy plate thick-layer rubber isolation bearing, a test bearing is made. Among them, the size of the connecting steel plate is 385 mm × 385 mm × 20mm; the thickness of the steel sealing plate is 12 mm, and the diameter is 250 mm; the thickness of the epoxy resin board for the reinforcement layer is 8 mm, with a diameter of 250 mm; the rubber layer has a thickness of 10.88 mm and a diameter of 250 mm. To obtain more accurate performance parameters of the bearing, while ensuring processing quality, three bearings of the same size and material were made for experimental research, and the average values of the horizontal and vertical stiffness of the three bearings were taken as the benchmark.

The epoxy plate thick-layer rubber isolation bearing specimen refers to the processing process of ordinary steel plate laminated rubber bearings. The epoxy resin plate coated with Kemlock adhesive is laminated with the rubber sheet, as shown in Figure 7. It is placed into the bearing mold and vulcanized using a high-temperature vulcanization device. The mold is shown in Figure 8, making the rubber and epoxy resin plate bonded together. Considering the high temperature resistance of the epoxy resin board and the thickness of the rubber layer, the vulcanization temperature of the epoxy rubber isolation bearing should be maintained within 138 ± 5 °C, with a vulcanization pressure of 8 MPa and a vulcanization time of 180 min. To ensure sufficient bonding between the epoxy resin board and the rubber, install the thick-layer rubber isolation bearing of the vulcanized epoxy board onto the connecting plate, as shown in Figure 9.

3.2.2. Experimental Loading Mechanism

1. Vertical mechanical performance test

The testing device adopts the YJW-20000 microcomputer controlled electro-hydraulic servo shear testing machine as shown in Figure 10. The loading method is shown in Figure 11. After loading the vertical pressure to the specified pressure value P_0, perform three cycles of loading (i.e., P_1, P_2) with ±30% P_0 amplitude changes. Finally, select the pressure value and vertical displacement obtained from the third load for vertical stiffness calculation. Use pressure sensors and displacement sensors to detect the vertical load and displacement values of the bearing, transfer the data to a computer, calculate the vertical stiffness, and take the average value. The vertical loading conditions are shown in Table 8.

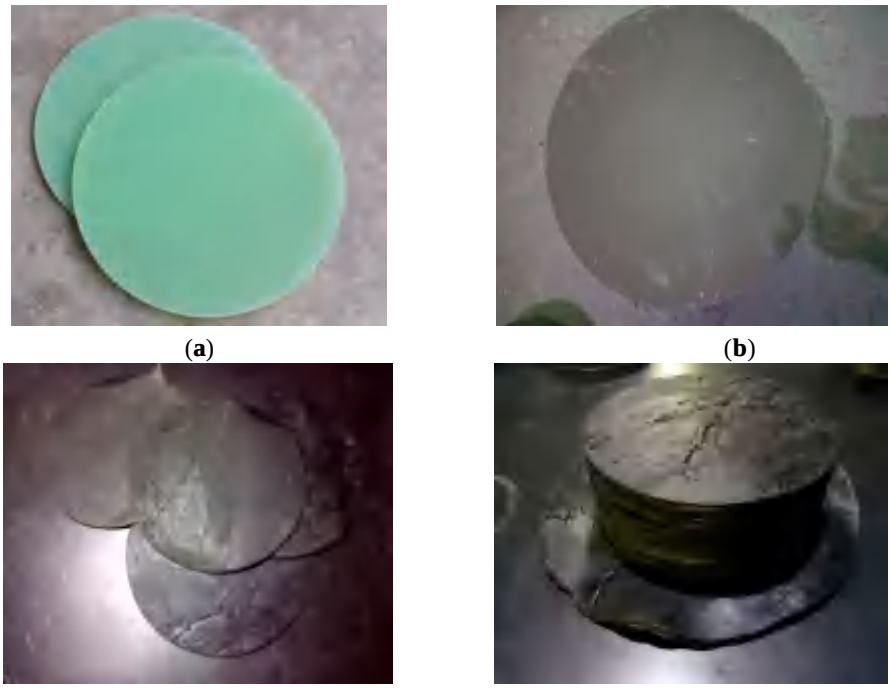

(**a**) (**b**)

(**c**) (**d**)

Figure 7. Epoxy resin board and rubber sheet. (**a**) Epoxy resin board; (**b**) Epoxy resin board after gluing; (**c**) Single layer rubber sheet; (**d**) Laminated rubber sheet.

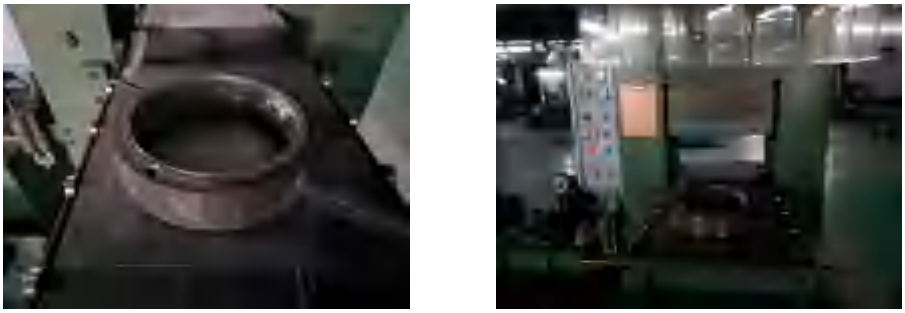

(**a**) (**b**)

Figure 8. High temperature vulcanization mold and device for bearing. (**a**) Mold; (**b**) Integrated device.

Figure 9. Epoxy resin board thick rubber isolation bearing.

Figure 10. YJW-20000 microcomputer controlled electro-hydraulic servo compression shear test machine.

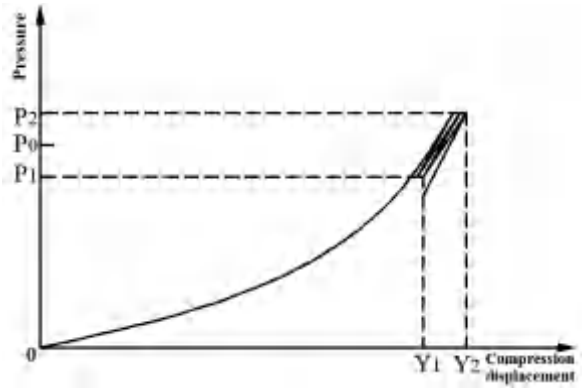

Figure 11. Vertical stiffness loading method.

Table 8. Vertical loading conditions of the bearing.

P_0 (kN)	Amplitude	Number of Cycles
75	±30%	3
150	±30%	3
200	±30%	3
300	±30%	3

After the completion of three cycles of loading, take the results of the third cycle of loading and calculate the vertical stiffness of the bearing according to the following formula:

$$K_v = \frac{P_2 - P_1}{Y_2 - Y_1} \quad (15)$$

P_1 and P_2: smaller pressure during the third cycle, kN;
Y_1 and Y_2: smaller pressure during the third cycle, mm.

2. Horizontal mechanical performance test

Horizontal performance tests were conducted on epoxy thick-layer rubber isolation bearings using different vertical pressures and shear displacements. The bearing is subjected to three cycles of sinusoidal loading, and the horizontal stiffness is calculated based on the test values of the third cycle. The horizontal loading conditions are shown in Table 9.

Table 9. Horizontal loading conditions of the bearing.

Shear Strain γ	Vertical Pressure (kN)	Loading Frequency (Hz)	Number of Cycles	Displacement (mm)
50%	75	0.02	3	49
	150	0.02	3	
	200	0.02	3	
	300	0.02	3	
100%	75	0.02	3	98
	150	0.02	3	
	200	0.02	3	
	300	0.02	3	

The restoring force model of epoxy thick-layer rubber isolation bearings is shown in Figure 12. Referring to the specifications and formulas [34], based on experimental data, the equivalent horizontal stiffness, equivalent damping ratio, post yield stiffness, and yield force of the bearings are obtained.

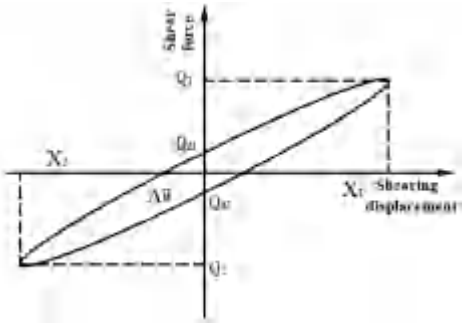

Figure 12. Restoration force model of epoxy plate thick layer rubber isolation bearing.

Equivalent horizontal stiffness:

$$K_h = \frac{Q_1 - Q_2}{X_1 - X_2} \tag{16}$$

Equivalent damping ratio:

$$h_{eq} = \frac{2\Delta W}{\pi K_h (X_1 - X_2)^2} \tag{17}$$

Post yield stiffness:

$$K_d = \frac{1}{2}\left(\frac{Q_1 - Q_{d1}}{X_1} + \frac{Q_2 - Q_{d2}}{X_2}\right) \tag{18}$$

Yield force:

$$Q_d = \frac{1}{2}(Q_{d1} - Q_{d2}) \tag{19}$$

Q_{d1}, Q_{d2}: the intersection point between the positive and negative directions of the hysteresis curve and the shear axis;

Q_1, Q_2: maximum and minimum shear force (kN);

ΔW: the envelope area of the hysteresis curve;

X_1: maximum displacement, $X_1 = T_1\gamma$;

X_2: maximum displacement, $X_2 = T_2(-\gamma)$.

According to the loading conditions of the vertical stiffness test of the bearing, the vertical stiffness test was conducted on the epoxy plate thick-layer rubber isolation bearing. The vertical compression test deformation of the bearing under different vertical pressures

is shown in Figure 13. Data were collected and different vertical pressure and displacement curves were plotted, as shown in Figure 14.

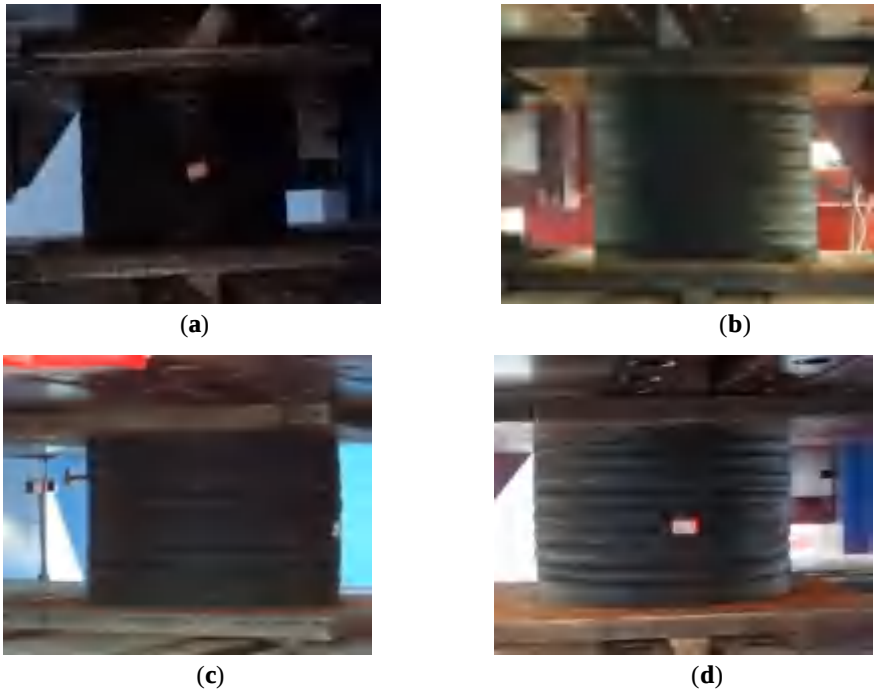

Figure 13. Compression test diagram of the bearing under different vertical pressures: (**a**) 75 kN; (**b**) 150 kN; (**c**) 200 kN; (**d**) 300 kN.

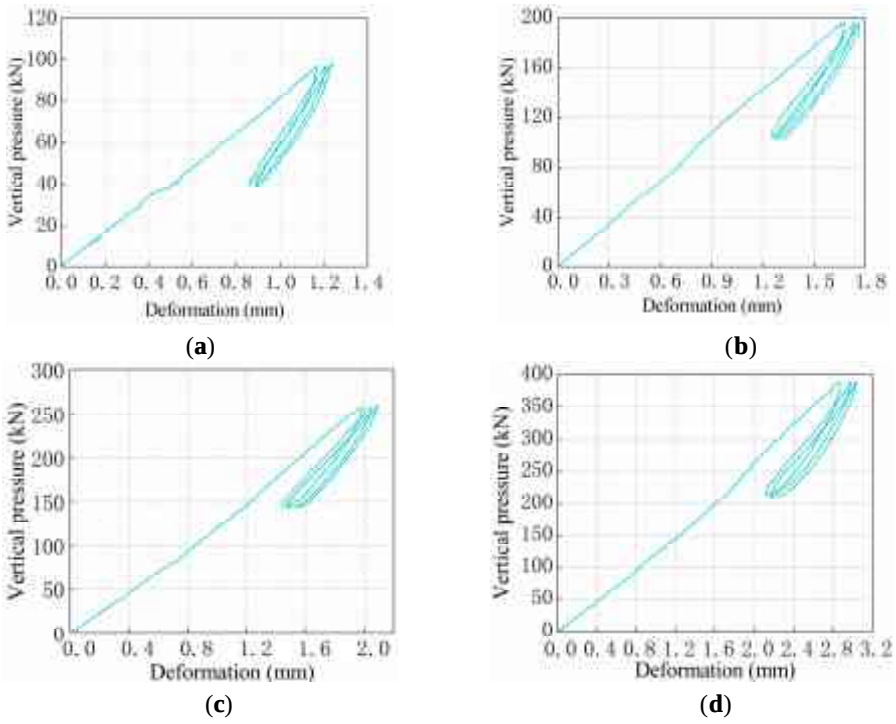

Figure 14. Vertical pressure–deformation curve of the bearing under different vertical pressures: (**a**) 75 kN; (**b**) 150 kN; (**c**) 200 kN; (**d**) 300 kN.

3.2.3. Analysis of Vertical Stiffness Test Results of Bearings and Correction of Calculation Formulas

1. Analysis of vertical stiffness test results

According to the loading conditions of the vertical stiffness test of the bearing, the vertical stiffness test was conducted on the epoxy plate thick-layer rubber isolation bearing. The vertical compression test deformation of the bearing under different vertical pressures is shown in Figure 13. Data were collected, and different vertical pressure and displacement curves were plotted as shown in Figure 14.

From Figure 13, it can be seen that under the vertical pressures of 75 kN, 150 kN, 200 kN, and 300 kN, each layer of rubber deforms and protrudes radially along the bearing, and the epoxy resin plate in the stiffening layer adheres firmly on the side without shedding, indicating good adhesion between the rubber and the epoxy resin plate, which meets the bonding strength requirements of the bearing in practical use. After experiencing different vertical pressures and multiple loads, the epoxy thick-layer rubber isolation bearing can still restore its original shape and has relatively stable deformation recovery ability.

As shown in Figure 14, the slope of the curve during the first cyclic loading is slightly smaller than that during the second and third loading, indicating that as the vertical deformation of the bearing increases, the vertical stiffness will gradually increase. According to Formula (15) for calculating the vertical stiffness of rubber isolation bearings, the vertical stiffness of the bearings is obtained, and the vertical stiffness curves of the bearing design and test are plotted as shown in Figure 15.

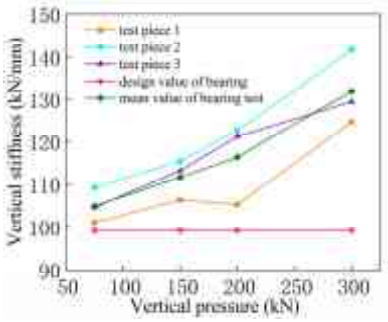

Figure 15. Design and test vertical stiffness of epoxy resin board thick rubber isolation bearing.

From Figure 15, it can be seen that there is a certain deviation between the vertical stiffness of the bearing obtained from the experiment and the design value, and it increases with the increase in vertical pressure, indicating that there is a significant deviation between the vertical stiffness test value of the epoxy plate thick-layer rubber isolation bearing and the standard design value.

2. Design vertical stiffness correction method

Under vertical pressure, the rubber layer of the epoxy plate thick rubber isolation bearing is compressed and deformed. The thickness of the rubber layer decreases, the cross-sectional area increases, and the rubber compression modulus increases. Therefore, it is necessary to consider the thickness of the rubber layer, the cross-sectional shape of the bearing, and the compression modulus of the rubber. The vertical stiffness of its design should be corrected using linear and integral methods. Figure 16 shows the analysis model of the uncompressed state of one layer of rubber.

(1) Linear correction method:

This method assumes that under vertical pressure, the thickness of the rubber layer after deformation of the rubber bearing decreases, but the cross-sectional dimensions of each height of the bearing remain constant, and the deformation is always cylindrical, as shown in Figure 17a. Based on the modified rubber modulus, analyze the influence of rubber layer thickness and cross-sectional area on the vertical stiffness of the bearing.

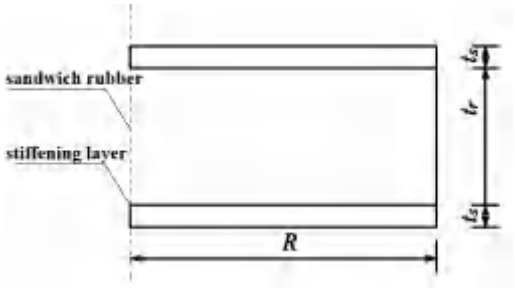

Figure 16. Analytical model of a layer of rubber uncompressed.

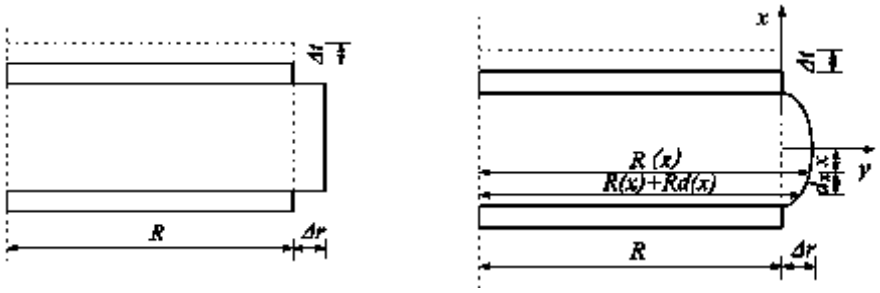

(**a**) (**b**)

Figure 17. Analytical model of a layer of rubber compression. (**a**) Linear; (**b**) Integral.

(2) Integral correction method:

This method considers the thickness of the rubber layer, the cross-sectional shape of the bearing, and the compressive modulus of the rubber. It is assumed that the shape of the lateral deformation of the bearing under vertical pressure satisfies the quadratic parabolic form shown in Figure 17b. Considering the incompressibility of rubber volume, assuming that the plane deformation is approximately equal, the relationship between horizontal deformation value Δr and vertical compression deformation Δt is as follows:

$$\Delta r = \frac{3R\Delta t}{4(t_r - \Delta t)} \tag{20}$$

t_r: initial thickness of single layer rubber;

R: initial radius of single-layer rubber.

According to the boundary conditions, the quadratic parabolic form of bearing deformation is obtained as follows:

$$y = -\frac{3R\Delta t}{(t_r - \Delta t)^3}x^2 + \frac{3R\Delta t}{4(t_r - \Delta t)} \tag{21}$$

The rubber radius at any thickness x of a single layer of rubber can be expressed as:

$$R(x) = R - \frac{3R\Delta t}{(t_r - \Delta t)^3}x^2 + \frac{3R\Delta t}{4(t_r - \Delta t)} \tag{22}$$

Considering the impact of volume changes on the performance of rubber under compression, the rubber bulk modulus E ∞ is introduced, and the compression elastic modulus of rubber is corrected according to the following equation.

$$E_c = E_0(1 + 2kS_1{}^2) \tag{23}$$

$$1/E_{cb} = 1/E_c + 1/E_\infty \tag{24}$$

E_0: is the elastic modulus;

k: It is an empirical coefficient.

Using numerical integration, the vertical stiffness k_v of the single-layer rubber is obtained, and then the overall vertical stiffness K_v of the bearing is obtained, where $A\ (x)$ is the cross-sectional area at position x.

$$\frac{1}{k_v(\Delta t)} = \int_{-\frac{t_r-\Delta t}{2}}^{\frac{t_r-\Delta t}{2}} \frac{1}{E_{cb}A(x)}d_x = \int_{-\frac{t_r-\Delta t}{2}}^{\frac{t_r-\Delta t}{2}} \frac{1}{E_{cb}\pi(R(x))^2}d_x \tag{25}$$

$$K_v = k_v/n \tag{26}$$

The linear correction method, integral correction method, and typical Lindley correction method were used to design and correct the vertical stiffness of the bearing under compression, and compared with the experimental values. As shown in Figure 18, under the vertical pressure of 75 kN, the deviation between the calculated value of the bearing vertical stiffness and the experimental value is mostly within 5%. As the vertical pressure increases, the error of the linear correction method gradually increases, while the integral correction method and Lindley correction method can well describe the process of strengthening the vertical stiffness of the bearing.

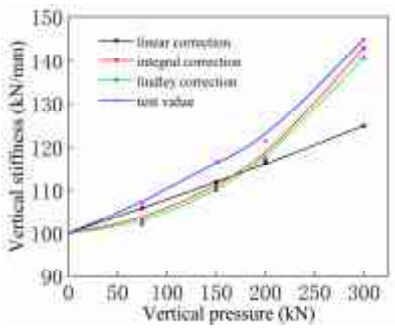

Figure 18. Comparison of vertical stiffness correction methods.

3.2.4. Experimental Results and Analysis of Horizontal Stiffness and Damping Ratio of Bearings

According to the loading conditions of the horizontal test, the horizontal performance of the epoxy plate thick-layer rubber isolation bearing is tested. The bearing compression shear tests at 50% and 100% shear strain under 300 kN are shown in Figure 19. As shown in Figure 19, under high vertical pressure, the deformation of each layer of rubber is relatively uniform, indicating that the deformation performance of its bearing is relatively stable under compression and shear. The shear strain versus displacement curves under different vertical pressures are shown in Figures 20 and 21.

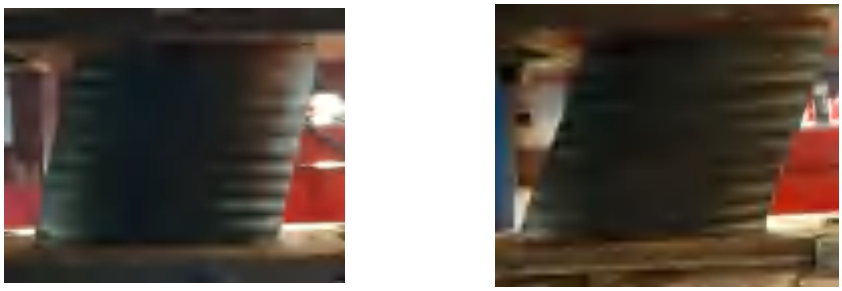

(**a**) (**b**)

Figure 19. Bearing horizontal performance test: (**a**) 50% shear strain; (**b**) 100% shear strain.

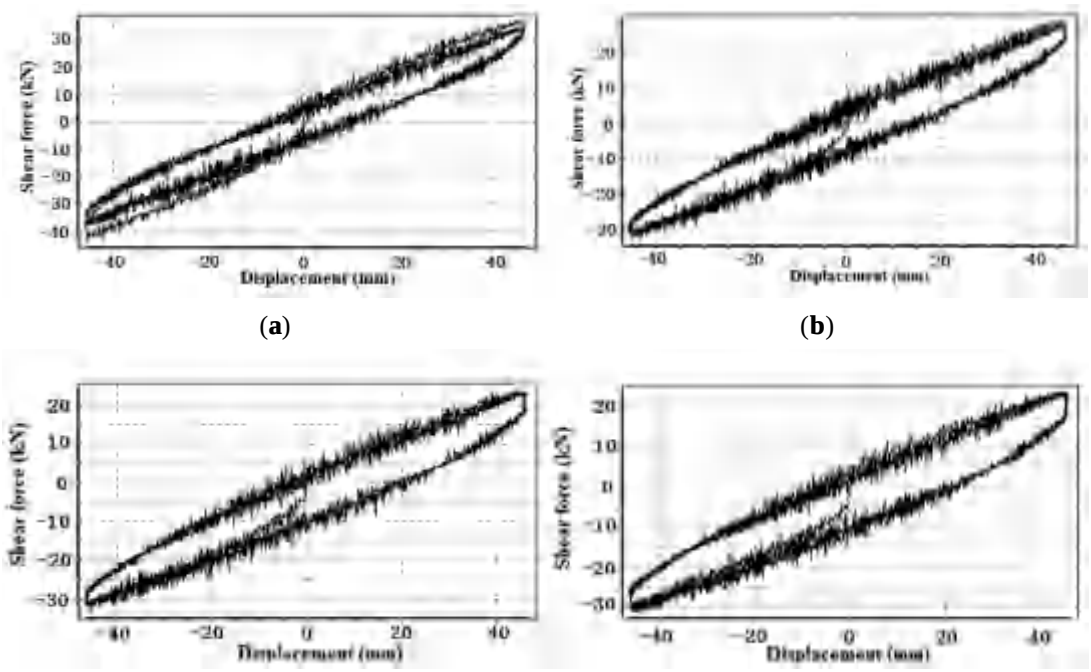

Figure 20. Shear displacement curve of epoxy plate thick-layer rubber isolation bearings under different vertical pressures under 50% shear strain: (**a**) 75 kN; (**b**) 150 kN; (**c**) 200 kN; (**d**) 300 kN.

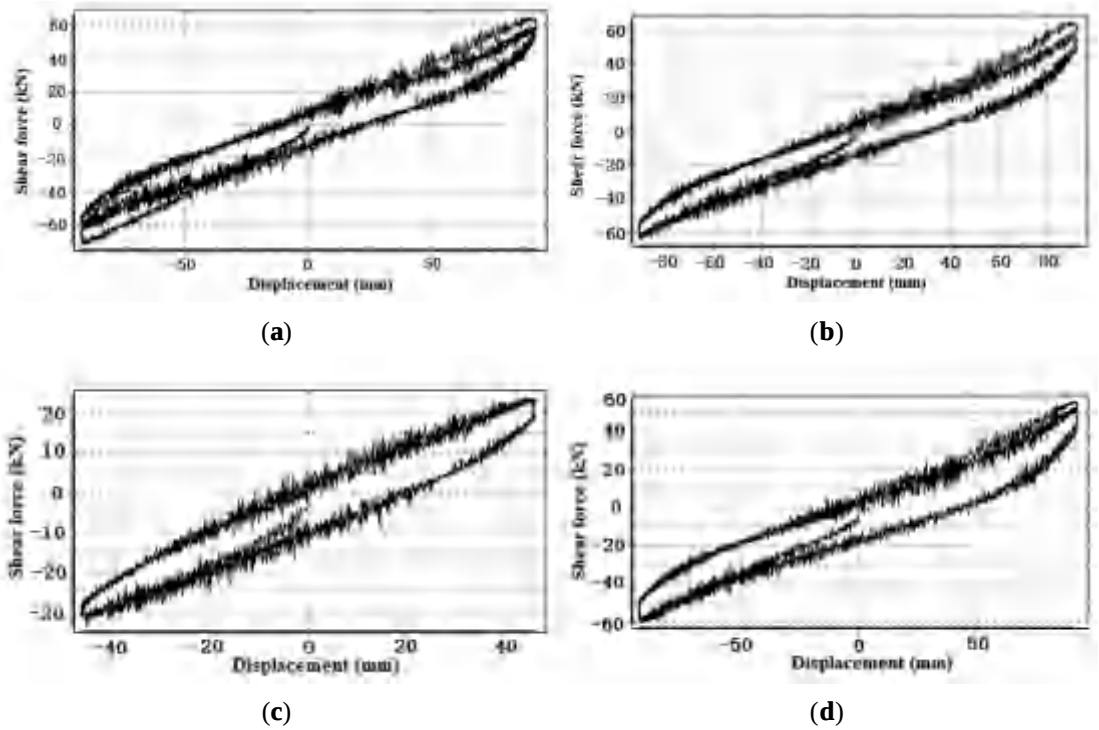

Figure 21. Shear displacement curve of epoxy plate thick-layer rubber isolation bearings under different vertical pressures under 100% shear strain: (**a**) 75 kN; (**b**) 150 kN; (**c**) 200 kN; (**d**) 300 kN.

As shown in Figure 20, as the vertical pressure increases, the envelope area of the shear displacement curve of the bearing gradually increases, and the saturation of the curve gradually increases, indicating that the damping of the bearing is affected by the vertical pressure, and the damping increases with the increase in the pressure value borne by the bearing. From Figure 21, it can be seen that when the shear displacement reaches

about 80 mm, the horizontal stiffness of the bearing undergoes stiffness strengthening, and the strengthening phenomenon becomes more pronounced with the increase in vertical pressure. It is beneficial to extend the natural vibration period of the structure, reduce the seismic response of the structure, and strengthen the stiffness of the bearing under large deformation, giving it greater horizontal stiffness, providing sufficient restoring force for the recovery of deformation of the bearing.

From Table 10 and Figure 22, it can be seen that when the shear strain of the epoxy plate thick rubber isolation bearing is constant, the horizontal equivalent stiffness of the bearing gradually decreases with the increase in vertical pressure, and the vertical stiffness of the bearing with 100% shear strain decreases faster, indicating that the shear deformation of the bearing has a more significant impact on its equivalent horizontal stiffness; from Table 10 and Figure 23, it can be seen that when the shear strain of the bearing is constant, the equivalent damping ratio gradually increases with the increase in its vertical pressure, and the equivalent damping ratio of the bearing at 50% shear strain is relatively large.

Table 10. Horizontal performance of epoxy resin board thick rubber isolation bearing.

Shear Strain γ	Vertical Pressure (kN)	Equivalent Horizontal Stiffness (kN/mm)	Equivalent Damping Ratio (%)	Post Yield Stiffness (kN/mm)
50%	75	0.66	9.1	0.64
	150	0.59	10.2	0.41
	200	0.55	11.4	0.36
	300	0.46	13.0	0.35
100%	75	0.62	8.3	0.43
	150	0.55	9.0	0.42
	200	0.50	9.7	0.36
	300	0.42	11.1	0.33

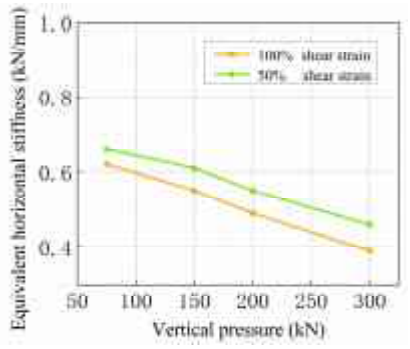

Figure 22. Curve of equivalent horizontal stiffness with vertical pressure.

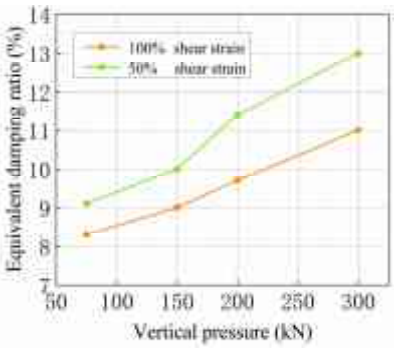

Figure 23. Curve of equivalent damping ratio with vertical pressure.

3.3. Finite Element Analysis of Epoxy Thick-Layer Rubber Isolation Bearings

3.3.1. Establishment of Finite Element Model

To verify the mechanical properties of epoxy thick-layer rubber isolation bearings, numerical simulations were conducted on oxygen thick-layer rubber isolation bearings using ABAQUS finite element software. The epoxy plate thick-layer rubber isolation support after grid division is shown in Figure 24, where the steel plate and FR-4 epoxy resin plate use C3D8 units, and the rubber uses C3D8H units and determine the Mooney–Rivlin parameters as shown in Table 11 based on the calculation formula of the rubber constitutive model in Section 2.1.4.

(**a**) (**b**)

Figure 24. Meshing of finite element model of epoxy resin board thick rubber isolation bearing. (**a**) Side view; (**b**) Vertical view.

Table 11. Mooney–Rivlin parameters for finite element simulation rubber.

Material Constitutive	Material Parameters (MPa)		C_{01}/C_{10}	Elastic Modulus $E = 6\ (C_{10} + C_{01})$ (MPa)	Shear Modulus $G = 2\ (C_{10} + C_{01})$ (MPa)
	C_{10}	C_{01}			
Mooney–Rivlin	0.40	0.10	0.25	3.00	1.00
Mooney–Rivlin	0.44	0.11	0.25	3.30	1.10
Mooney–Rivlin	0.48	0.12	0.25	3.60	1.20
Mooney–Rivlin	0.52	0.13	0.25	3.90	1.30

3.3.2. Verification of Finite Element Model of Bearing

1. Horizontal stiffness of bearing

By applying vertical pressures of 75 kN, 150 kN, 200 kN, and 300 kN to the thick-layer rubber isolation bearing of the epoxy board, the shear strain was loaded with 50% and 100% amplitude, respectively. Set the loading frequency of the bearing to 0.02 Hz to obtain the horizontal stiffness of the bearing under different pressures and shear deformations. The relationship between the horizontal stiffness of the bearing and vertical pressure is shown in Figure 25. The greater the vertical pressure, the faster the horizontal stiffness decreases. The error between the simulated horizontal stiffness and experimental stiffness of the bearing under different vertical pressures is less than 5%, and the simulation results are more accurate.

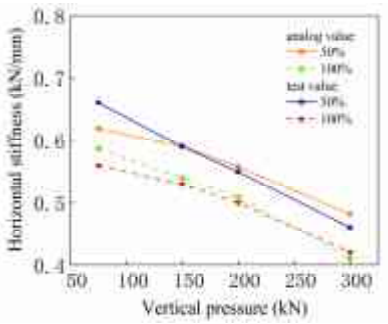

Figure 25. Correlation between horizontal stiffness and shear strain.

2. Vertical stiffness of bearing

When the shear strain is 0, the vertical stiffness of the epoxy plate thick-layer rubber isolation bearing is obtained based on different vertical pressures, as shown in Figure 26. From Figure 26, it can be seen that as the vertical pressure increases, the vertical stiffness of the epoxy thick-layer rubber isolation bearing increases. When the vertical pressure of the rubber bearing is less than 200 kN, the error between the simulated value and the experimental value is less than 6%.

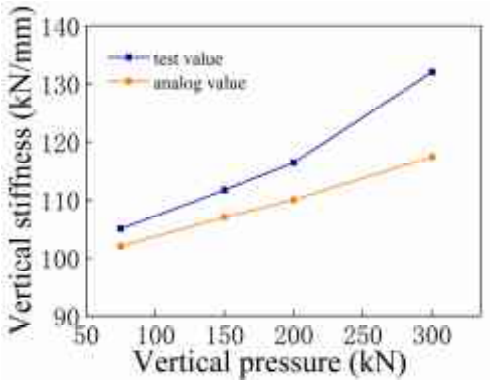

Figure 26. Correlation between vertical stiffness and vertical pressure.

3.3.3. Stress Analysis of Bearing Stiffening Layer (Epoxy Resin Board) under Different Shear Deformations

Under the vertical pressure of 75 kN, the epoxy plate thick-layer rubber isolation bearing is subjected to 50%, 100%, and 175% shear strain sinusoidal loading along the horizontal direction, respectively, to obtain the stress distribution of the bearing under compression and shear, as shown in Figure 27.

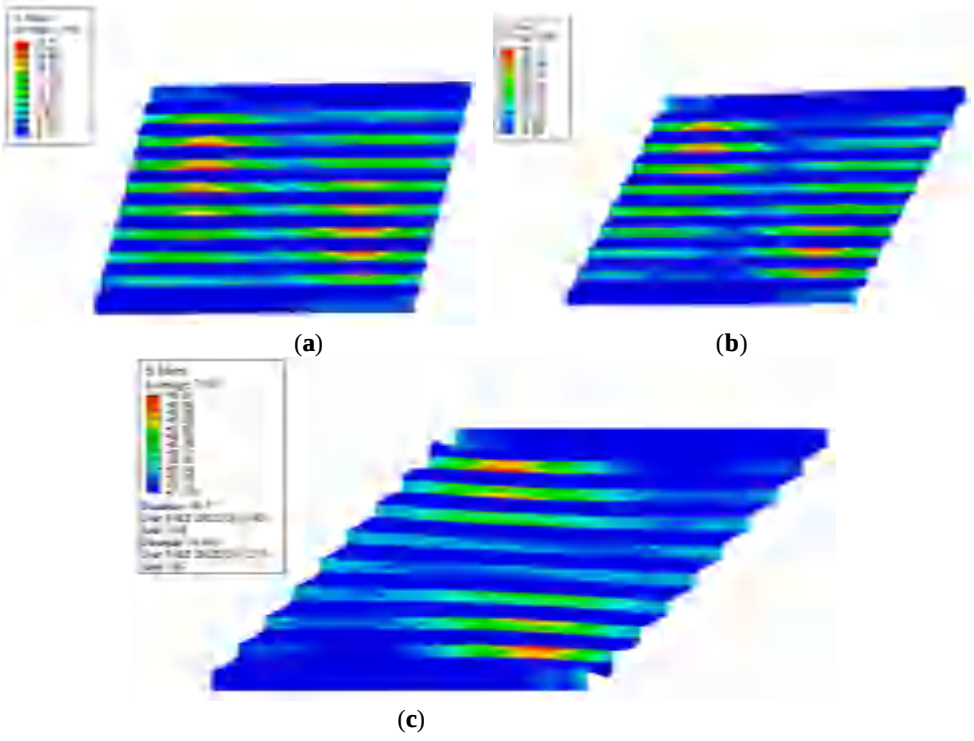

Figure 27. Mises stress distribution under different shear strains of the bearing: (**a**) 50% shear strain; (**b**) 100% shear strain; (**c**) 175% shear strain.

The relationship between the maximum stress of the reinforced epoxy board and the shear strain of the bearing is shown in Figure 28. Under the same vertical pressure, when the shear strains are 50%, 100%, and 175%, the maximum stress values of the reinforced epoxy board are 29.95 MPa, 56.92 MPa, and 93.87 MPa, respectively, which are much smaller than the material strength of the epoxy board. As the shear strain of the bearing increases, the stress borne by the epoxy resin board gradually increases, and the stress value increases faster with the increase in shear strain.

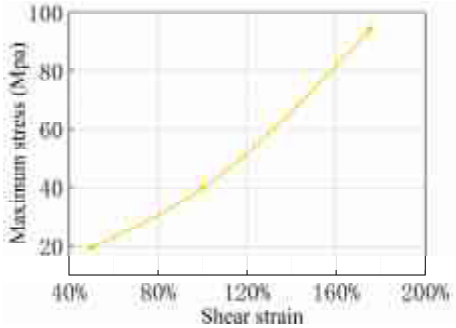

Figure 28. Relationship between the maximum stress of the epoxy layer of the stiffener and the shear strain of the bearing.

Taking the vertical pressure of 75 kN and 50% shear strain of the bearing as an example, the stress distribution of the 1st, 3rd, 5th, and 7th layers of epoxy resin plate thick-layer rubber isolation bearings was obtained, as shown in Figure 29.

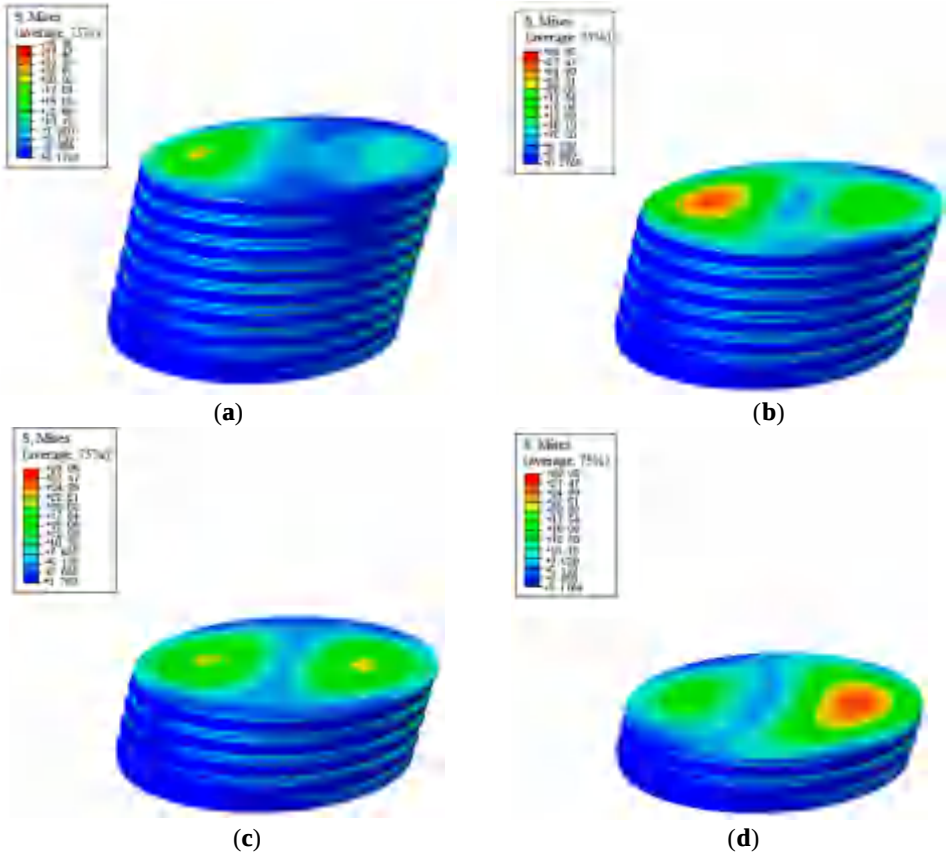

Figure 29. Sectional stress distribution of each layer of epoxy board at 50% shear strain under the action of 75 kN. (**a**) Layer 1; (**b**) Layer 3; (**c**) Layer 5; (**d**) Layer 7.

As shown in Figure 29, the horizontal section stress of the epoxy resin board of the bearing is symmetrically distributed, with the maximum concentrated stress mainly distributed at a distance of 60mm from the center of the epoxy resin board. With the maximum stress as the center, the stress gradually decreases in all directions. Under the vertical pressure of 75 kN, the thick-layer rubber isolation bearing of epoxy resin plate establishes a path through the center of the epoxy resin plate circle and the center position in the thickness direction based on different shear strains of the bearing. The stress path output for the 1st, 3rd, 5th, and 7th layers of the epoxy resin plate is shown in Figure 30.

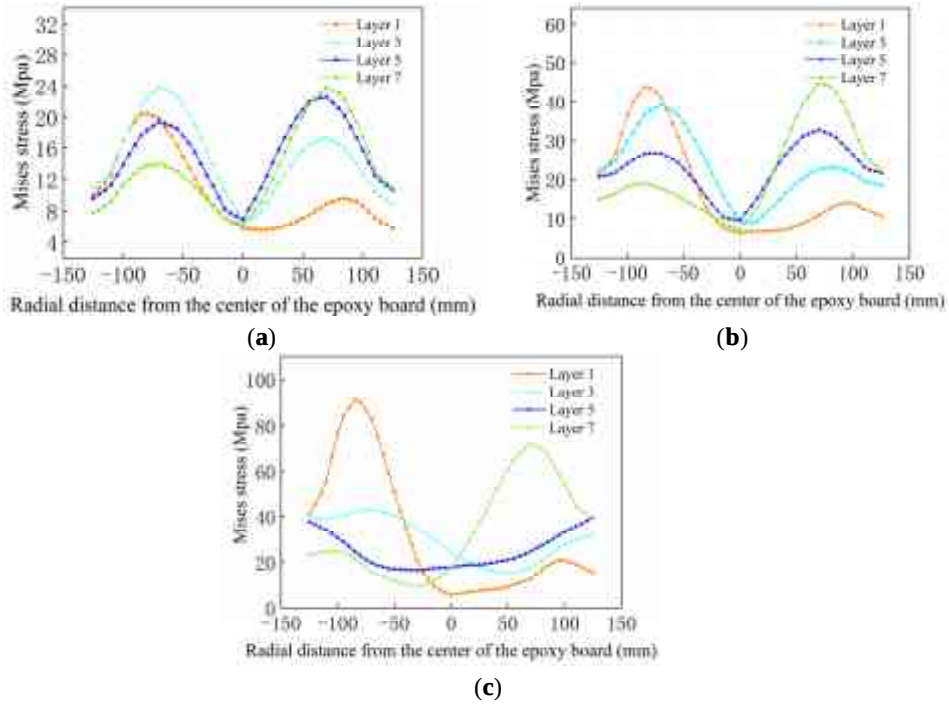

Figure 30. Stress distribution of epoxy resin sheet in the stiffening layer of the bearing under different shear strains: (**a**) 50% shear strain; (**b**) 100% shear strain; (**c**) 175% shear strain.

From Figure 30, it can be seen that the first and seventh layers of epoxy resin plates bear the maximum stress, which increases with the increase in shear strain. The results show that the stress near the upper and lower sealing plates of epoxy resin plates is the highest, and the material strength of this area should be carefully considered when designing bearings.

4. Conclusions

The orthogonal design method and efficiency coefficient method were used to optimize the design of epoxy thick-layer rubber isolation bearings, and the mechanical properties of the bearings were tested and numerically simulated. The following conclusions were drawn:

(1) The epoxy plate thick-layer rubber isolation bearing has smaller horizontal shear deformation and horizontal stiffness, which is beneficial for extending the natural vibration period of the structure and reducing its seismic response, the strengthening of the stiffness of the bearing under large deformation gives it greater horizontal stiffness, providing sufficient restoring force for the recovery of deformation of the bearing, which is conducive to dissipating the energy transmitted by earthquakes during the use of the support.

(2) Under vertical pressure, the deviation between the calculated value of the vertical stiffness of the bearing and the experimental value is small. As the vertical pressure increases, the error of the linear correction method gradually increases, while the

integral correction method and Lindley correction method can effectively describe the process of strengthening the vertical stiffness of the bearing.

(3) According to the stress distribution law of the epoxy board inside the bearing under different vertical pressures and shear deformations, the stress of the epoxy resin board is mainly concentrated on the upper and lower sides of the board. As the shear deformation increases, the stress concentration position gradually moves towards the top and bottom of the bearing, and the stress value also increases.

It is worth noting that in the design and analysis of epoxy thick-layer rubber isolation bearings, it is crucial to choose suitable isolation bearing materials. Epoxy plates and rubber materials should have good weather resistance, corrosion resistance, and wear resistance. Consideration should also be given to the construction and maintenance of the bearing to ensure its easy installation, easy maintenance and replacement, and the impact of temperature on the bearing. The above suggestions can help engineers consider some important factors in the design and analysis of epoxy thick-layer rubber isolation bearings, ensuring the reliability, safety, and economy of the bearings.

Author Contributions: Conceptualization, Q.P. and Z.X.; methodology, Q.P. and P.Q.; validation, Q.P., Z.X. and P.Q.; formal analysis, Y.Z. and P.Q.; investigation, Y.Z., Q.P. and Z.X.; data curation, Y.Z., J.Z. and Z.X.; writing—original draft preparation, P.Q. and Q.P.; writing—review and editing, Q.P. and P.Q.; supervision, Z.X., Y.Z. and J.Z.; project administration, Y.Z., Z.X. and J.Z.; formal analysis, Y.Z., J.Z. and Z.X.; funding acquisition, Z.X. All authors have read and agreed to the published version of the manuscript.

Funding: This research was supported by the University Characteristic Innovation Project of Guangdong Province Education Foundation (grant no. 2019KTSCX102), Dalian University Research Platform Project (202301ZD01), the National Natural Science Foundation of China (grant nos. 51878108 and 51478168), the Natural Science Research Project of Guangdong University of Petrochemical Technology (grant no. 519192) and the Department of Science and Technology Guidance Plan Foundation of Liaoning Province (grant no. 2019JH8/10100091).

Data Availability Statement: The data used to support the findings of this study are available from the corresponding author upon request.

Conflicts of Interest: The authors declare no conflict of interest.

References

1. Pei, Q.; Qi, P.F.; Ma, F.H.; Cui, D.; Xue, Z.C.; Ding, Y. Resistance of Gable Structure of Nuclear Island to Progressive Collapse in Conventional Island Shield Building of Nuclear Power Plants. *Buildings* **2023**, *13*, 1257. [CrossRef]
2. Pei, Q.; Cai, B.W.; Zhang, L.X.; Xue, Z.C.; Qi, P.F.; Cui, D.; Wang, X.T. The Progressive Collapse Resistance Mechanism of Conventional Island Shield Buildings in Nuclear Power Plants. *Buildings* **2023**, *13*, 958. [CrossRef]
3. Markou, G.; Genco, F. Seismic assessment of small modular reactors: NuScale case study for the 8.8 Mw earthquake in Chile. *Nucl. Eng. Des.* **2018**, *12*, 176–204. [CrossRef]
4. Chen, J.Y.; Zhao, C.F.; Xu, Q.; Yuan, C.Y. Seismic analysis and evaluation of the base isolation system in AP1000 NI under SSE loading. *Nucl. Eng. Des.* **2014**, *7*, 117–133. [CrossRef]
5. Sayed, M.A.; Go, S.; Cho, S.G.; Kim, D. Seismic responses of base-isolated nuclear power plant structures considering spatially varying ground motions. *Struct. Eng. Mech.* **2015**, *54*, 169–188. [CrossRef]
6. Ali, A.; Hayah, N.A.; Kim, D.; Cho, S.G. Design response spectra-compliant real and synthetic GMS for seismic analysis of seismically isolated nuclear reactor containment building. *Nucl. Eng. Technol.* **2017**, *49*, 825–837. [CrossRef]
7. Hou, G.L.; Li, M.; Hai, S.; Song, T.S.; Wu, L.S.; Li, Y.; Zheng, G.; Shen, F.; Chen, Y.D. Innovative seismic resistant structure of shield building with base isolation and tuned-mass-damping for AP1000 nuclear power plants. *Eng. Comput.* **2019**, *36*, 1238–1257. [CrossRef]
8. Whittaker, A.S.; Sollogoub, P.; Kim, M.K. Seismic isolation of nuclear power plants: Past, present and future. *Nucl. Eng. Technol.* **2018**, *7*, 290–299. [CrossRef]
9. Kim, H.S.; Ju, O. A Study on Isolation Performance of High Damping Rubber Bearing Through Shaking Table Test and Analysis. *J. Korea Acad.-Ind. Coop. Soc.* **2016**, *17*, 601–611. [CrossRef]
10. Bhuiyan, A.R.; Alam, M.S. Seismic performance assessment of highway bridges equipped with superelastic shape memory alloy-based laminated rubber isolation bearing. *Eng. Struct.* **2012**, *11*, 396–407. [CrossRef]
11. Gu, Z.Y.; Feng, L.; Sun, Y.; Gong, H.; Zhu, C.H.; Chen, Z.J.; Dai, J.Q.; Hao, F.Z.; Zhong, X.T.; Qian, W.P. Seismic Response Analysis of a Large-Span Isolated Structure Equipped with TNRB-DSBs and LRBs. *Buildings* **2023**, *13*, 1288. [CrossRef]

12. Liu, Y.H.; Zhang, J.J.; Huang, X.Y.; Xue, S.T. Seismic Performance of Building with Novel Steel Roller Isolation Bearing: Experimental and Numerical Studies. *J. Earthq. Eng.* **2022**, *27*, 2119–2144. [CrossRef]
13. Weisman, J.; Warn, G.P. Stability of Elastomeric and Lead-Rubber Seismic Isolation Bearings. *J. Struct. Eng.* **2012**, *138*, 214–222. [CrossRef]
14. Hou, G.L.; Liu, Y.; Li, M.; Sun, M.H.; Sun, F.; Zhu, X.Y.; Pan, R.; Zhang, D.Y. Seismic structural responses reduction of double-layered containment nuclear power plant via BIS-TMD. *Eng. Comput.* **2020**, *37*, 2111–2125. [CrossRef]
15. Kumar, M.; Whittaker, A.S.; Constantinou, M.C. Extreme earthquake response of nuclear power plants isolated using sliding bearings. *Nucl. Eng. Des.* **2017**, *316*, 9–25. [CrossRef]
16. Pan, P.; Shen, S.D.; Shen, Z.Y.; Gong, R.H. Experimental investigation on the effectiveness of laminated rubber bearings to isolate metro generated vibration. *Measurement* **2017**, *122*, 554–562. [CrossRef]
17. Wu, P.S.; Ou, J.P. Performance Analysis and Comparison of Two Base Isolation Systems with Super-Large Displacement Friction Pendulum Bearings. *Appl. Sci.* **2020**, *10*, 8325. [CrossRef]
18. Zou, X.G.; Yang, W.G.; Liu, P.; Wang, M. Shaking table tests and numerical study of a sliding isolation bearing for the seismic protection of museum artifacts. *J. Build. Eng.* **2022**, *65*, 105725. [CrossRef]
19. Zhu, X.Y.; Pan, R.; Li, J.B.; Lin, G. Study of isolation effectiveness of nuclear reactor building with three-dimensional seismic base isolation. *Eng. Comput.* **2020**, *39*, 1209–1233. [CrossRef]
20. Peng, T.B.; Guan, J.Y.; Wu, Y.C. Numerical and Experimental Investigation of the Seismic Effect of a Two-Stage Seismic Isolation Method. *Sustainability* **2023**, *15*, 4883. [CrossRef]
21. Liang, Q.H.; Luo, W.L.; Zhou, Y.; Ke, X.B.; Li, J.R. Seismic performance of a novel three-dimensional isolation bearing. *J. Build. Eng.* **2022**, *57*, 104818. [CrossRef]
22. Zhang, H.D.; Liang, X.; Gao, Z.Y.; Zhu, X.Q. Seismic performance analysis of a large-scale single-layer lattice dome with a hybrid three-directional seismic isolation system. *Eng. Struct.* **2020**, *214*, 110627. [CrossRef]
23. Han, Q.H.; Jing, M.; Lu, Y.; Liu, M.J. Mechanical behaviors of air spring-FPS three-dimensional isolation bearing and isolation performance analysis. *Soil Dyn. Earthq. Eng.* **2021**, *149*, 106872. [CrossRef]
24. Zhang, Z.; Niu, M.Q.; Yuan, K.; Zhang, Y.W. Research on linear/nonlinear viscous damping and hysteretic damping in nonlinear vibration isolation systems. *Appl. Math. Mech.-Engl. Ed.* **2020**, *41*, 983–998. [CrossRef]
25. Wang, Y.; Zhu, X.H.; Zheng, R.; Tang, Z.; Chen, B.B. Analysis and design of the power law damping based on the nonlinear vessel isolation system. *Adv. Mech. Eng.* **2019**, *10*, 1687814018817194. [CrossRef]
26. Kang, X.F.; Li, S.; Hu, J. Design and Parameter Optimization of the Reduction-Isolation Control System for Building Structures Based on Negative Stiffness. *Buildings* **2023**, *13*, 489. [CrossRef]
27. Mofidian, S.M.M.; Bardaweel, H. Displacement transmissibility evaluation of vibration isolation system employing nonlinear-damping and nonlinear-stiffness elements. *J. Vib. Control* **2018**, *24*, 4247–4259. [CrossRef]
28. Shi, S.J.; Zhou, P.Z.; Lu, Z.H.; Du, J.B. Design Synthesis of Vibration Isolation System Considering Host Structure, Damping Layer, and Resilient Mounts. *J. Vib. Eng. Technol.* **2022**, *11*, 2037–2055. [CrossRef]
29. Zhang, Y.M.; Li, J.W.; Wang, L.B.; Wu, H. Study on the Seismic Performance of Different Combinations of Rubber Bearings for Continuous Beam Bridges. *Adv. Civ. Eng.* **2020**, *2020*, 8810874. [CrossRef]
30. Yuan, Y.; Wei, W.; Ni, Z.B. Analytical and experimental studies on an innovative steel damper reinforced polyurethane bearing for seismic isolation applications. *Eng. Struct.* **2021**, *239*, 112254. [CrossRef]
31. Peng, J.; Li, Y.F. Seismic Analysis of Reticulated Shell Structure Based on Sensor Network for Smart Transportation Seismic Isolation Bearings. *J. Adv. Transp.* **2022**, *2022*, 5985542. [CrossRef]
32. Anas, S.M.; Alam, M.; Umair, M. Experimental and numerical investigations on performance of reinforced concrete slabs under explosive-induced air-blast loading: A state-of-the-art review. *Structures* **2021**, *31*, 428–461. [CrossRef]
33. Anas, S.M.; Alam, M.; Umair, M. Air-blast and ground shockwave parameters, shallow underground blasting, on the ground and buried shallow underground blast-resistant shelters: A review. *Int. J. Prot. Struct.* **2021**, *13*, 99–139. [CrossRef]
34. Architectural Institute of Japan. *Recommendation for the Design of Base Isolated Buildings*; Seismological Press: Beijing, China, 2006.
35. Lan, Z.Y. *Comparative Study on Static and Dynamic Performance of Lead Rubber Isolation Bearings*; Guangzhou University: Guangzhou, China, 2016.
36. *GB/T 20688.1-2007*; Rubber Bearings—Part 1: Seismic-Protection Isolators test Methods. China Standards Publishing House: Beijing, China, 2007.
37. *GB/T 7760-2003*; Rubber, Vulcanized or Thermoplastic—Determination of Adhesion to a Rigid Substrate—90 Degrees Peel Method. China Standards Publishing House: Beijing, China, 2003.
38. *GB/T 20688.3-2006*; Rubber Bearings—Part 3: Elastomeric Seismic-Protection Isolators for Buildings. China Standards Publishing House: Beijing, China, 2007.
39. *JG/T118-2018*; Rubber Isolation Bearings for Buildings. China Standards Publishing House: Beijing, China, 2018.